

Circumstellar SiO masers in the long-period variable star TX Cam

R. Soria-Ruiz*

Joint Institute for VLBI in Europe

E-mail: soria@jive.nl

F. Colomer

Observatorio Astronómico Nacional, Apartado 112, E-28803 Alcalá de Henares, Spain

E-mail: f.colomer@oan.es

J. Alcolea

Observatorio Astronómico Nacional, Alfonso XII 3, E-28014 Madrid, Spain

E-mail: j.alcolea@oan.es

V. Bujarrabal

Observatorio Astronómico Nacional, Apartado 112, E-28803 Alcalá de Henares, Spain

E-mail: v.bujarrabal@oan.es

J.-F. Desmurs

Observatorio Astronómico Nacional, Alfonso XII 3, E-28014 Madrid, Spain

E-mail: jf.desmurs@oan.es

K. B. Marvel

American Astronomical Society, 2000 Florida Avenue NW Suite 400, Washington, DC

20009-1231, USA

E-mail: marvel@aas.org

We present the latest results of a multi-line study of SiO circumstellar masers in oxygen-rich AGB stars using the VLBA. In particular, we have studied several maser lines at 43 GHz ($\nu=1$ and $\nu=2$) and at 86 GHz ($\nu=1$ and $\nu=2$) of ^{28}SiO , and for the first time we have been able to map the emission of the ground state $\nu=0$ $J=1-0$ of ^{29}SiO and the $\nu=2$ $J=2-1$ maser line of ^{28}SiO . In TX Cam, the 3-mm emission is produced in an outer region of the circumstellar envelope, as it has been already observed in other late-type stars. We also discuss the importance of these new detections in the framework of the SiO maser pumping models.

The 8th European VLBI Network Symposium

September 26-29, 2006

Toruń, Poland

*Speaker.

1. Introduction

Circumstellar SiO maser emission is mainly detected in evolved stars. This peculiar emission is produced at a few stellar radii from the central star, in the innermost shells of the circumstellar envelopes formed due to the mass loss process occurring while in the AGB phase. Among other properties, it is well established that the SiO maser emission appears distributed in ring structures composed of many compact spots with sizes of a few milliarcseconds, and very high brightness temperatures, therefore being an ideal target for VLBI studies. On the other hand, the maser amplification is shown in ^{28}SiO , ^{29}SiO and ^{30}SiO in many rotational transitions, which have been extensively studied with single-dish observations. Thanks to those observations, we know some important properties associated to the SiO circumstellar maser emission, as for example, the correlation with the IR $8\mu\text{m}$ stellar radiation or its time variability [1]. In this paper, we present the latest results obtained in a multi-epoch and multi-transition study of the SiO maser emission in AGB stars.

2. Observations and results

High-resolution observations of R Leo and TX Cam were carried out with the NRAO¹ VLBA in October 2001 and December 2002. A summary of the ^{28}SiO and ^{29}SiO maser transitions studied is shown in Table 1. The data were correlated in Socorro. The array setup let us achieve a maximum angular resolution of 0.17 and 0.12 milliarcseconds at 43 GHz and 86 GHz respectively (see Table 1). The calibration was done following the standard procedures for spectral line VLBI described in the *AIPS cookbook*². The maps were produced using the CLEAN deconvolution algorithm. All the presented figures were made using the GILDAS software³.

In TX Cam, the ^{29}SiO lines were not detected and the ^{28}SiO $\nu=1$ $J=2-1$ data could not be calibrated due to very weak emission of the phase calibrator. The results for R Leo will be presented elsewhere. A more detailed description of the maps obtained for TX Cam is given in the subsequent section.

3. Relative spatial distribution

The main objective of these simultaneous observations was to study the relative spatial distribution of the SiO maser emissions. Depending on the excitation energy, the maser lines require different physical and chemical conditions. For example, the emissions in the $\nu=1$ and $\nu=2$ vibrational states are separated by about 2000 K, and therefore, are expected to be located in different regions of the envelope. This comparison of the masing layers is often used to constrain the current pumping models. In fact, there is still a big debate whether the mechanism that pumps the SiO circumstellar masers is the infrared stellar radiation or the collisions with gas particles.

Our results for TX Cam seem to be in good agreement with previous studies of oxygen-rich stars. When comparing the 43-GHz lines, $J=1-0$, the $\nu=2$ emission is produced in an inner part of

¹The National Radio Astronomy Observatory is a facility of the National Science Foundation operated under cooperative agreement by Associated Universities, Inc.

²<http://www.aoc.nrao.edu/aips/cook.html>

³<http://www.iram.fr/IRAMFR/GILDAS>

Table 1: Summary of observational results for TX Cam

SiO maser transition	frequency (MHz)	bandwidth (MHz)	number of channels	resolution (km s ⁻¹)	restoring beam (miliarcsecond) (first & second epoch)	
²⁸ SiO $\nu=1$ $J=1-0$	43122.080	8	256	0.22	0.54×0.43	0.73×0.61
$\nu=2$ $J=1-0$	42820.587	8	256	0.22	0.44×0.17	0.26×0.16
²⁹ SiO $\nu=0$ $J=1-0$	42879.916	8	256	0.22	————	————
²⁸ SiO $\nu=1$ $J=2-1$	86243.442	16	512	0.11	————	0.34×0.22
$\nu=2$ $J=2-1$	85640.456	16	512	0.11	————	0.68×0.32
²⁹ SiO $\nu=0$ $J=2-1$	85759.132	16	512	0.11	————	————

the envelope (Figures 1 and 2). In the first epoch, the spatial distribution of the maser spots was similar (Figure 1). The angular diameters and separation of the masing regions are compatible with the measurements made by [3] and [9]. However, in the second run, the ring distribution is less clear and the profiles differ, but there are some features appearing in both transitions. We note that the intensity of the emission and the line profiles vary from one epoch to the other. Nevertheless, this latter facts and the disruption in the ring morphology have been observed in the monitoring of the $\nu=1$ $J=1-0$ maser line in TX Cam by [4].

On the other hand, the angular size of the 86-GHz $\nu=1$ $J=2-1$ region is larger than the $J=1-0$ one (see Figure 3). We confirm the results found in other evolved stars, IRC+10011 and R Leo (see [6], [7] and [8]). In addition, we have been able to map for the first time the $\nu=2$ $J=2-1$ maser emission in an oxygen-rich AGB star. One maser component has been mapped, thus making difficult to derive any spatial information, and the line is weak if we compare it to the other masers. The infrared line overlap was firstly proposed by [5] to explain the quenching of the $\nu=2$ $J=2-1$ emission in oxygen variables. Further calculations by [2], [6] and [8] have shown that the conditions of the excitation of the SiO molecule change drastically when the line overlaps are introduced in the model calculations, and therefore also their relative spatial distribution.

References

- [1] Alcolea, J., & Bujarrabal, V. 1992, A&A, 253, 475
- [2] Bujarrabal, V., Alcolea, J., Sánchez Contreras, C., & Colomer, F. 1996, A&A, 314, 883
- [3] Desmurs, J.-F., Bujarrabal, V., Colomer, F., & Alcolea, J. 2000, A&A, 360, 189
- [4] Diamond, P. J., & Kemball, A. J. 2003, ApJ, 599, 1372
- [5] Olofsson, H., Hjalmarsen, A., & Rydbeck, O.E.H. 1981, A&A, 100, L30
- [6] Soria-Ruiz, R., Alcolea, J., Colomer, F., Bujarrabal, V., Desmurs, J.-F., Marvel, K. B. & Diamond, P. J. 2004, A&A, 426, 131
- [7] Soria-Ruiz, R., Colomer, F., Alcolea, J., Bujarrabal, V., Desmurs, J.-F. & Marvel, K. B. 2005, A&A, 432, L39
- [8] Soria-Ruiz, R., *PhD Thesis*, Universidad Autónoma de Madrid, 2006
- [9] Yi, J., Booth, R. S., Conway, J. E. & Diamond, P. J. 2005, A&A, 432, 531

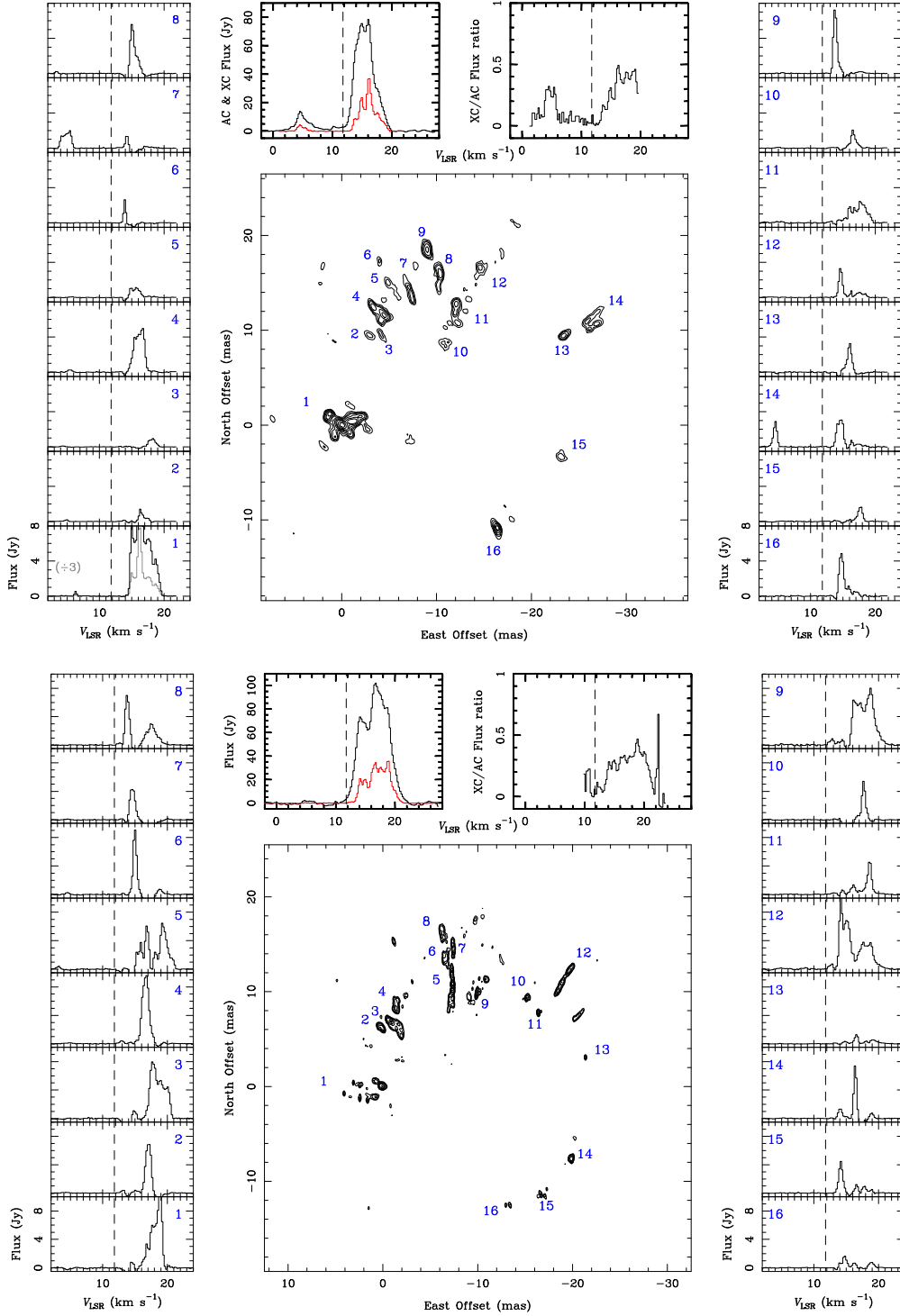


Figure 1: The ^{28}SiO $\nu=1$ (upper figure) and $\nu=2$ $J=1-0$ (lower figure) maser transition in TX Cam. These plots show the integrated intensity map in $\text{Jy beam}^{-1} \text{ km s}^{-1}$ units (center panel), the spectrum of the maser spots that appear on the map (numbered boxes), the total power spectrum (black) and recovered flux (red) in the map (left panel above the map), and the ratio of these magnitudes (right panel above the map). The dashed vertical lines mark the systemic velocity of the source, $V_{\text{LSR}}=11.8 \text{ km s}^{-1}$. For the $\nu=1$ line, the peak intensity is $6.50 \text{ Jy beam}^{-1} \text{ km s}^{-1}$, the contour levels are 0.17, 0.18, 0.19, 0.38, 0.77, 1.55, 3.12 and $6.25 \text{ Jy beam}^{-1} \text{ km s}^{-1}$, and the *rms* is $0.05 \text{ Jy beam}^{-1} \text{ km s}^{-1}$. In the case of the $\nu=2$ line, the peak intensity is $3.91 \text{ Jy beam}^{-1} \text{ km s}^{-1}$, the contour levels are 0.39, 0.43, 0.47, 0.96, 1.91 and $3.90 \text{ Jy beam}^{-1} \text{ km s}^{-1}$, and the *rms* is $0.08 \text{ Jy beam}^{-1} \text{ km s}^{-1}$.

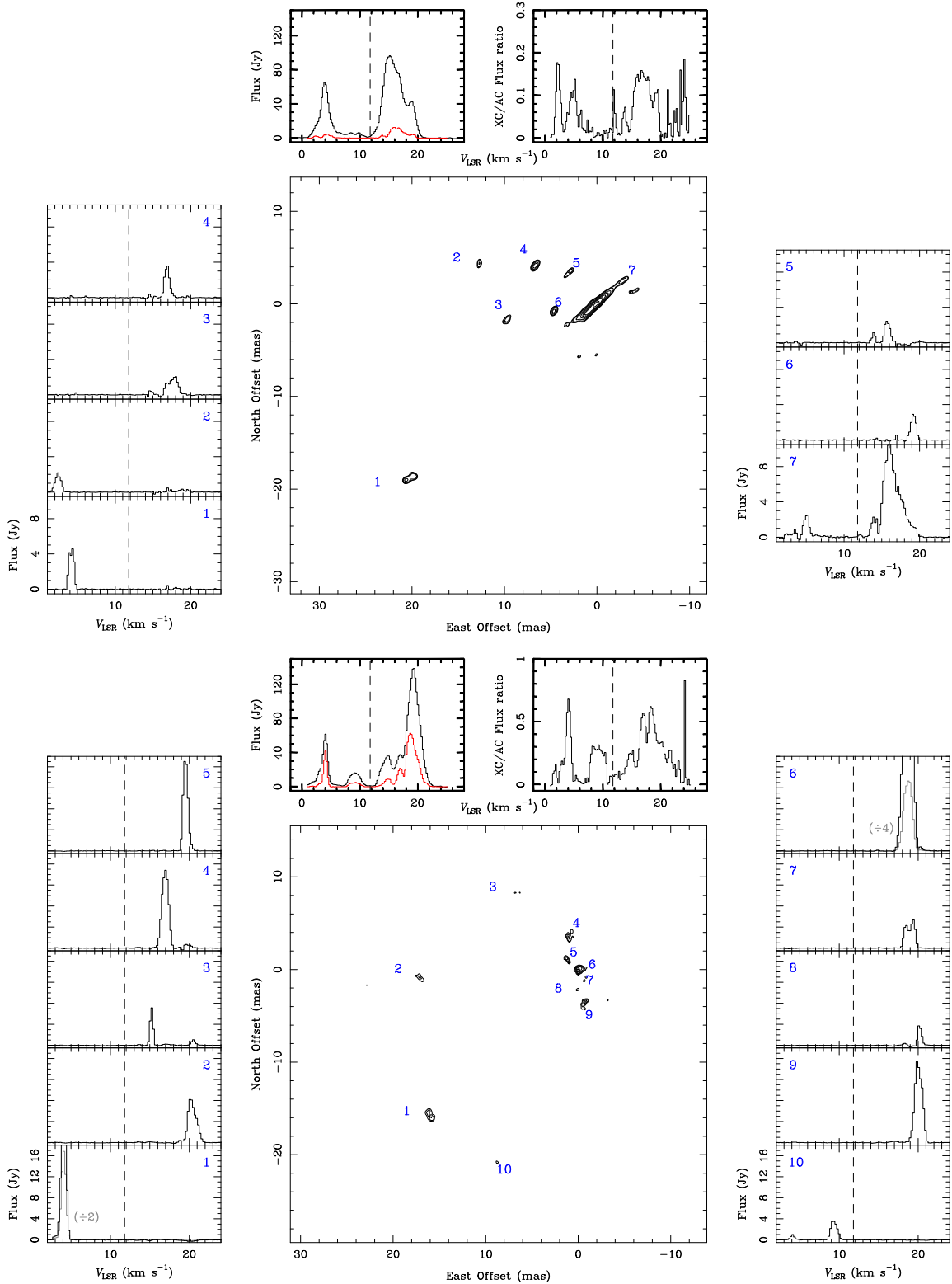


Figure 2: Same as Figure 1 but for the second epoch observed in TX Cam. For the $\nu=1$ line, the peak intensity is $2.99 \text{ Jy beam}^{-1} \text{ km s}^{-1}$, the contour levels are 0.69, 0.75, 0.89, 1.19, 1.49, 1.79, 2.09 and $2.69 \text{ Jy beam}^{-1} \text{ km s}^{-1}$, and the rms is $0.03 \text{ Jy beam}^{-1} \text{ km s}^{-1}$. In the $\nu=2$ map, the peak intensity is $15.65 \text{ Jy beam}^{-1} \text{ km s}^{-1}$, the contour levels are 0.47, 0.96, 1.91, 3.82, 7.65 and $15.31 \text{ Jy beam}^{-1} \text{ km s}^{-1}$, and the rms is $0.02 \text{ Jy beam}^{-1} \text{ km s}^{-1}$.

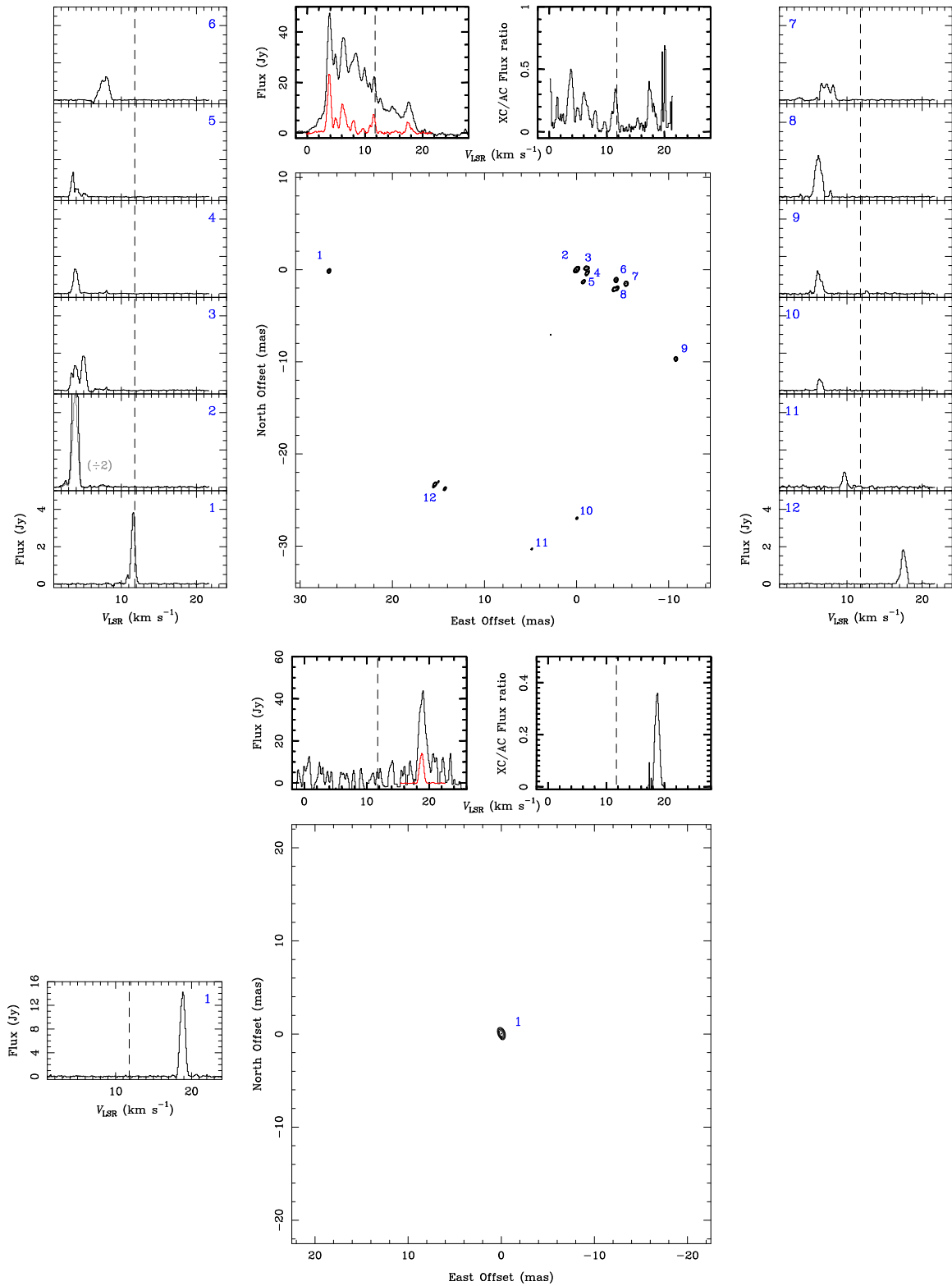


Figure 3: Same as Figure 1 but for the ^{28}SiO $\nu=1$ (upper plot) and $\nu=2$ (lower plot) $J=2-1$ in TX Cam. For the $\nu=1$ line, the peak intensity is $4.09 \text{ Jy beam}^{-1} \text{ km s}^{-1}$, the contour levels 0.16, 0.22, 0.28, 0.38, 0.48, 0.97, 1.95 and $3.90 \text{ Jy beam}^{-1} \text{ km s}^{-1}$, and the *rms* is $0.02 \text{ Jy beam}^{-1} \text{ km s}^{-1}$. For the $\nu=2$, the maximum intensity is $5.07 \text{ Jy beam}^{-1} \text{ km s}^{-1}$, the contours are 0.31, 0.62, 1.24, 2.48 and $4.96 \text{ Jy beam}^{-1} \text{ km s}^{-1}$, and the *rms* is $0.03 \text{ Jy beam}^{-1} \text{ km s}^{-1}$.